



Kinetic, equilibrium, and thermodynamic studies of heavy metal removal from aqueous solutions by natural material from Morocco

Adil Ksakas¹ · Abdellah Arrahli² · Abdelaziz Dra¹ · Fahoul Youssef¹ · Iboustaten Elmustafa¹ · Abdelali El Gaidoumi³ · Karim Tanji¹ · Abdelhak Kherbeche¹

Received: 29 October 2021 / Accepted: 28 February 2022 / Published online: 26 March 2022
© Springer Nature Switzerland AG 2022

Abstract

This study deals with the adsorption kinetics, equilibrium, and thermodynamics of the removal of Cr(VI) and Cu(II) ions from an aqueous solution using natural material from Morocco (NMT). The adsorbent used is characterized by different physicochemical techniques such as X-ray fluorescence spectrometry, X-ray diffraction (XRD), Fourier transform infrared spectroscopy (FTIR), scanning electron microscopy (SEM), and energy-dispersive X-ray spectroscopy (EDX). The effects of various experimental conditions, including contact time, pH, adsorbent dosage, initial concentration, and temperature, on metal removal by the natural adsorbent were investigated. Under optimal conditions, adsorption efficiencies of 65.21% and 91.31% are respectively observed for Cr(VI) and Cu(II) ions, and the adsorption is explained well by the pseudo-second-order kinetic model. The experimental equilibrium adsorption data were analyzed using the Langmuir, Freundlich, and Dubinin–Radushkevich (D–R) isotherm equations at different concentrations. The Langmuir separation factor R_L and the n value for the Freundlich isotherm show that Cr(VI) and Cu(II) ions are adsorbed favorably onto the NMT. Thermodynamic parameters, such as the Gibbs free energy (ΔG), the adsorption entropy (ΔS), and the adsorption enthalpy (ΔH), suggest that the adsorption process is spontaneous, endothermic, and controlled by physical mechanisms for both heavy metals.

Keywords Chromium · Copper · Adsorption · Kinetic · Natural adsorbent

Introduction

The use of natural materials for heavy metal removal has become a concern in all countries. Moreover, there is heavy metal contamination in the aqueous waste streams from many industries, such as metal plating facilities and mining (Riffi and Hte 2013). Chemical industry wastewaters polluted with heavy metal ions represent a hazard to all living

organisms, especially humans (Abou Zakhem and Hafez 2015).

Adsorption is defined as a phenomenon that occurs between the surface of a solid and a fluid and leads to enrichment of the fluid density at the solid–fluid interface. Due to its simple principle, it has been widely used in the field of wastewater treatment, and the availability of an extensive range of adsorbents is one of the strengths of this method (Booker et al. 1996; Olusegun et al. 2018; Kamagate et al. 2018; Qu et al. 2020). It is also regarded as one of the most efficient methods for the removal of toxic and nonbiodegradable compounds such as heavy metals (Motsi et al. 2009; Burakov et al. 2018).

Solid materials with high adsorption capacities have a porous structure like a sea sponge, and their adsorption capacities are determined by the radius and number of these pores (Copaja et al. 2020). Natural materials that are available in large quantities or certain wastes from agricultural processes may have the potential to be used as low-cost adsorbents, as they represent unused resources (Šćiban et al. 2007; Jeguirim and Limousy 2019; El Mrabet et al. 2020),

Communicated by Aymen Amin Assadi, Associate Editor.

✉ Karim Tanji
karim.tanji@usmba.ac.ma

¹ Laboratory of Materials, Catalysis and Environment, Higher School of Technology, Fès, Morocco

² Euromed Research Center, International Institute of Applied Sciences, Euro-Mediterranean University of Fez, Fès, Morocco

³ École Supérieure de Technologie de Khénifra, Université Sultan Moulay Slimane, Béni Mellal, Morocco

are widely available, and are environmentally friendly. Various materials such as natural zeolites, lignocellulosic materials, waste tires, biomaterials, industrial wastes, agricultural wastes, and clay minerals are used as adsorbents for the removal of heavy metals (Annadurai et al. 2003; Bohli et al. 2017). Clay minerals are a group of phyllosilicates with small sizes—typically less than 2 μm in their longest dimension. In addition, clays have been used for thousands of years and are still among the most important industrial materials. They have also been used for chemical studies for various purposes, including the adsorption of various organic and inorganic substances, radioactive specimens, and heavy metals (Saltali et al. 2007; Uddin 2017; Gao et al. 2020).

The aim of the work presented in this paper was to remove chromium and copper ions from an aqueous solution using a natural material called NMT from the oriental area of Morocco. The effects of contact time, solution pH, adsorbent dosage, initial concentration of ions, and temperature on the adsorption efficiency were investigated in batch experiments. The kinetic, equilibrium, and thermodynamic parameters were investigated using experimental data to describe the adsorption process (Veli et al. 2007; Pholosi et al. 2020).

Materials and methods

Materials

The NMT was collected from a local oriental area of Morocco. It was crushed and sieved to produce a distribution of particles with sizes of less than 63 μm before being used for the adsorption study (Amar et al. 2021).

All of the reagents were analytical grade (Sigma–Aldrich) and were used as received without any further treatment. Various Cr(VI) solutions with concentrations ranging from 25 to 250 mg L^{-1} and from 250 mg L^{-1} to 1750 mg L^{-1} were prepared by dissolving $\text{K}_2\text{Cr}_2\text{O}_7 \cdot 2\text{H}_2\text{O}$ (98%) and copper(II) nitrate trihydrate $[\text{Cu}(\text{NO}_3)_2 \cdot 3\text{H}_2\text{O}]$ (99.99%) in distilled water at room temperature, respectively. Sodium hydroxide (0.5 mol L^{-1}) and hydrochloric acid (0.5 mol L^{-1}) solutions were used to adjust the solution pH (Dra et al. 2020a, b; Gao et al. 2020; El Gaidoumi et al. 2021).

Methods

Characterizations

Several physicochemical techniques were used to characterize the NMT: X-ray diffraction using an X'Pert Pro diffractometer with an X'Celerator high-speed detector equipped with a copper anticathode ($l = 1.5418 \text{ \AA}$), X-ray fluorescence spectrometry (Oxford MDX1000), scanning electron

microscopy and energy-dispersive X-ray spectroscopy (EDX) using a Quanta 200 scanning electron microscope equipped with an EDAX probe, and Fourier transform (FT) infrared (IR) spectroscopy using a Vertex 70 instrument. Conductivity was measured by inoLab Level 2 laboratory conductivity meters, and the pH was measured using a PHS-3E pH-meter. The concentrations of Cr(VI) and Cu(II) ions were determined according to the Beer–Lambert law (Tournassat et al. 2015) by UV–visible spectrophotometry using a VR-2000 instrument. Table 1 shows some physicochemical properties of the NMT (Assila et al. 2021; Jeguirim and Limousy 2019; Campodonico et al. 2015).

Kinetic and equilibrium studies

The kinetics and equilibrium of the adsorption of heavy metals by the adsorbent sample were studied in batch experiments. For this, 1 g of the adsorbent sieved at 40 μm was added to 200 mL of a metal ion solution in a 500 mL glass beaker at room temperature under magnetic stirring (250 rpm) (Bayuo et al. 2020). During the experimental studies, the contact time was varied from 5 to 400 min. After the agitation period, the suspension was filtered through filter paper (0.45 μm pore size), and the supernatant was analyzed by UV–vis spectrophotometry.

The percentage of heavy metal ions adsorbed was calculated using the equation

$$\text{Removal}(\%) = \frac{([C]_0 - [C]_t)}{[C]_0} \times 100, \quad (1)$$

where C_0 and C_t are the concentration of metal ions initially and at time t , respectively (Bayuo et al. 2020).

After each adsorption test, the adsorbent was separated from the solution by centrifugation and filtered through 0.45 μm paper filter to eliminate any particles before being analyzed by the spectrophotometer (Fig. 1).

In this study, the effects of several factors such as pH [ranging from 2 to 6 for Cu(II) ions and from 2 to 10 for Cr(VI); the pH of the solution was adjusted with dilute 0.5 M HCl or 0.5 M NaOH solution], the initial concentration of the solution, the amount of adsorbent (ranging from

Table 1 Physicochemical properties of the NMT

Adsorbent	pH	Conductivity ($\mu\text{S/cm}$)	Specific surface area BET ($\text{m}^2 \text{g}^{-1}$)	Granulometry (μm)
NMT	8.74	88.74	11.12	63

BET Brunauer, Emmett, and Teller

1 to 10 g L⁻¹), and the contact time on the metal ion removal efficiency were examined (Panda et al. 2011).

The equilibrium amount of metal adsorbed from aqueous solution was determined from the following equation:

$$q_e = \frac{([C]_0 - [C]_e)}{m \times V}, \quad (2)$$

where q_e (mg g⁻¹) is the equilibrium adsorption capacity, C_0 (mg L⁻¹) is the initial concentration of the adsorbate, C_e (mg L⁻¹) is the equilibrium concentration of the adsorbate, V (L) is the volume of the solution, and m (g) is the adsorbent amount (Jeguirim and Limousy 2019; Wang et al. 2017).

Results and discussion

Adsorbent characterization

X-ray fluorescence spectrometry

The quantitative analysis carried out on the NMT adsorbent using X-ray fluorescence spectrometry (XRF) (Oxford MDX1000) showed that the NMT adsorbent contains significant amounts of calcium oxide (32.57%) and quartz (31.13%) (Table 2) (Dra et al. 2019; Panda et al. 2011).

Figure 2 shows plots of the surface area and pore volume of the NMT adsorbent versus the relative pressure, measured using a Micromeritics ASAP2420 system. The

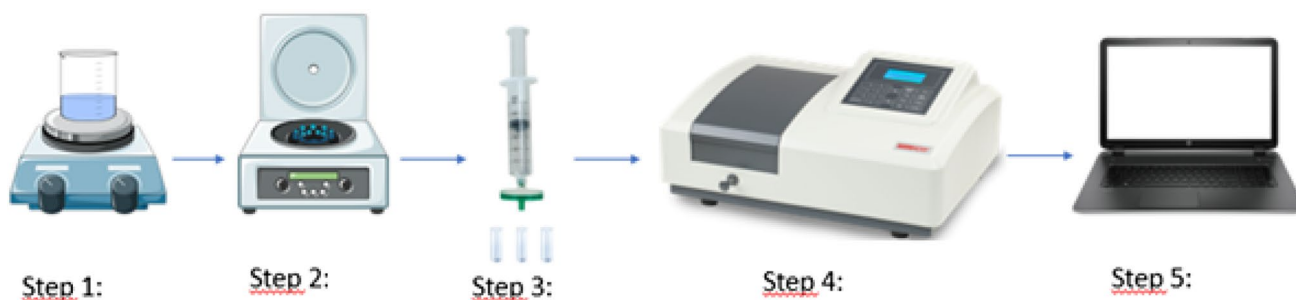


Fig. 1 Steps involved in the filtration of the metal solutions

Table 2 Chemical composition of the NMT

Compound	SiO ₂	Al ₂ O ₃	Fe ₂ O ₃	CaO	MgO	SO ₃	K ₂ O	Na ₂ O	Loss on ignition
Weight percentage	31.13	3.10	0.68	32.57	0.88	0.11	0.95	0.00	29.45

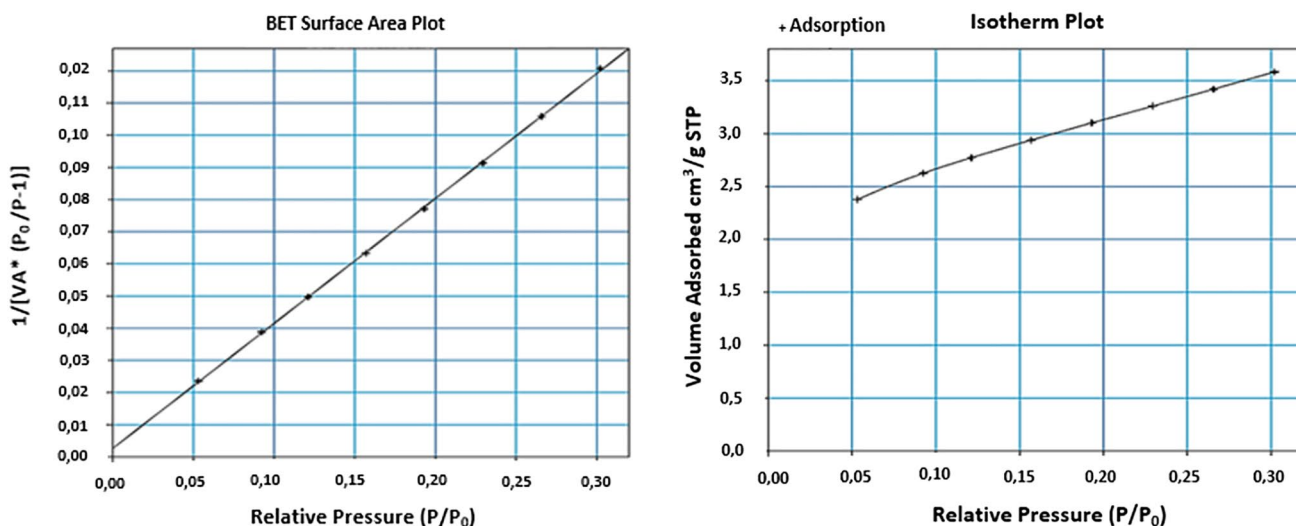


Fig. 2 BET surface area of the NMT adsorbent

plots show that NMT has a surface area of $11 \text{ m}^2 \text{ g}^{-1}$ and a pore volume of $2.55 \text{ cm}^3 \text{ g}^{-1}$.

X-ray diffraction (XRD)

A diffractogram of the natural material is presented in Fig. 3. The diffractogram indicates the presence of calcite (CaCO_3) and silica quartz (SiO_2). The large quantity of CaO (32.52%) present according to the X-ray fluorescence results is due to the presence of a significant quantity of CaCO_3 in the NMT (Dehmani et al. 2020; Wang et al. 2021; Magali 2008).

Fourier transform infrared spectroscopy

Figure 4 shows the infrared spectrum (IR) of the NMT. It shows the main absorption bands that are characteristic of calcite: two intense vibrational bands from C–O stretching are observed at 1405 cm^{-1} and 871 cm^{-1} , and there is a less intense band from C–O at 712 cm^{-1} . The band at 1010 cm^{-1} represents asymmetric stretching vibrations of Si–O–Si, while the band at 796 cm^{-1} is due to symmetric vibrations of Si–O–Si. Quartz Si–O stretching vibration bands were found at 469 and 525 cm^{-1} . These results confirm the presence of the quartz previously observed in the XRD diffractogram (Dra et al. 2020a, b; Dra et al. 2019).

Fig. 3 X-ray diffractogram of the NMT (C calcite, Q quartz)

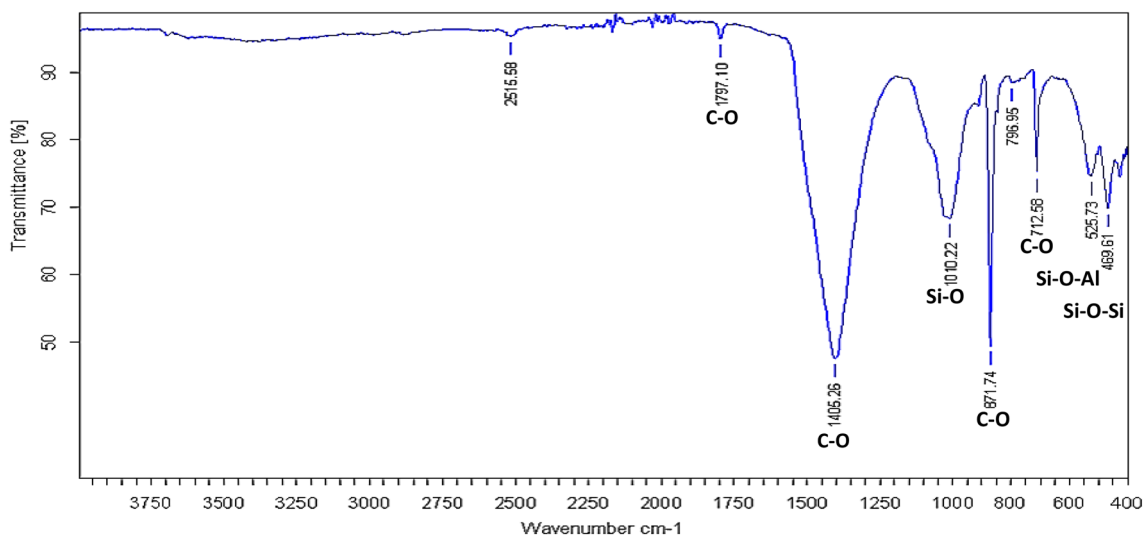
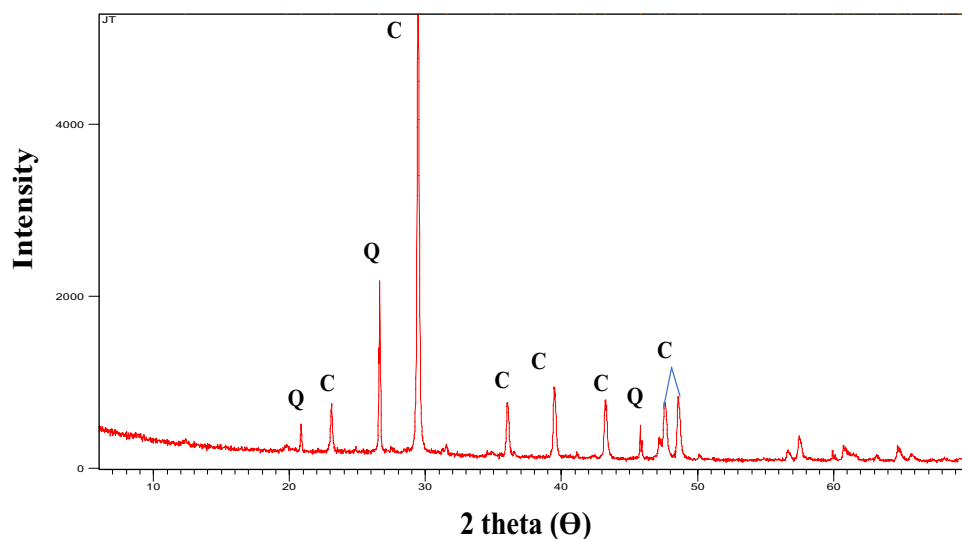


Fig. 4 FTIR spectrum of the NMT

Scanning electron microscopy and energy-dispersive X-ray spectroscopy

A scanning electron microscope (SEM) was used to check the solid morphology and average crystal size of the natural material, as shown in Fig. 5. As observed in the SEM images, NMT particles are mostly irregular in shape and have porous surfaces (Assila et al. 2021; Campodonico et al. 2015).

Kinetic and equilibrium studies

Effect of contact time

Figure 6 presents the effect of contact time on the removal of Cr(VI) and Cu(II) ions by the NMT. The effect of contact time was investigated in the range from 5 min to 6 h. It was

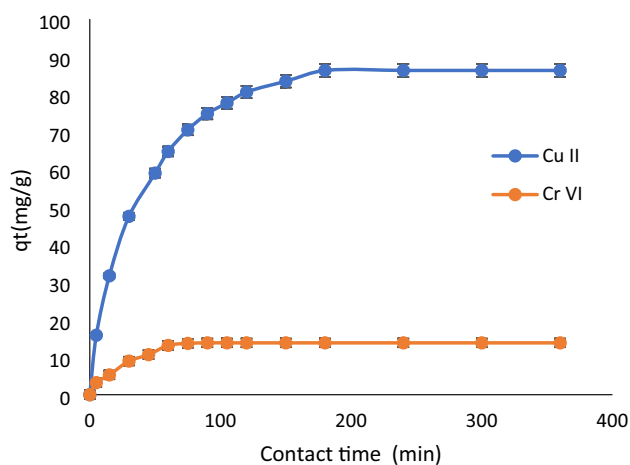


Fig. 6 Effect of contact time on the adsorption capacity q (mg g^{-1}) of NMT for Cr(VI) and Cu(II) ions

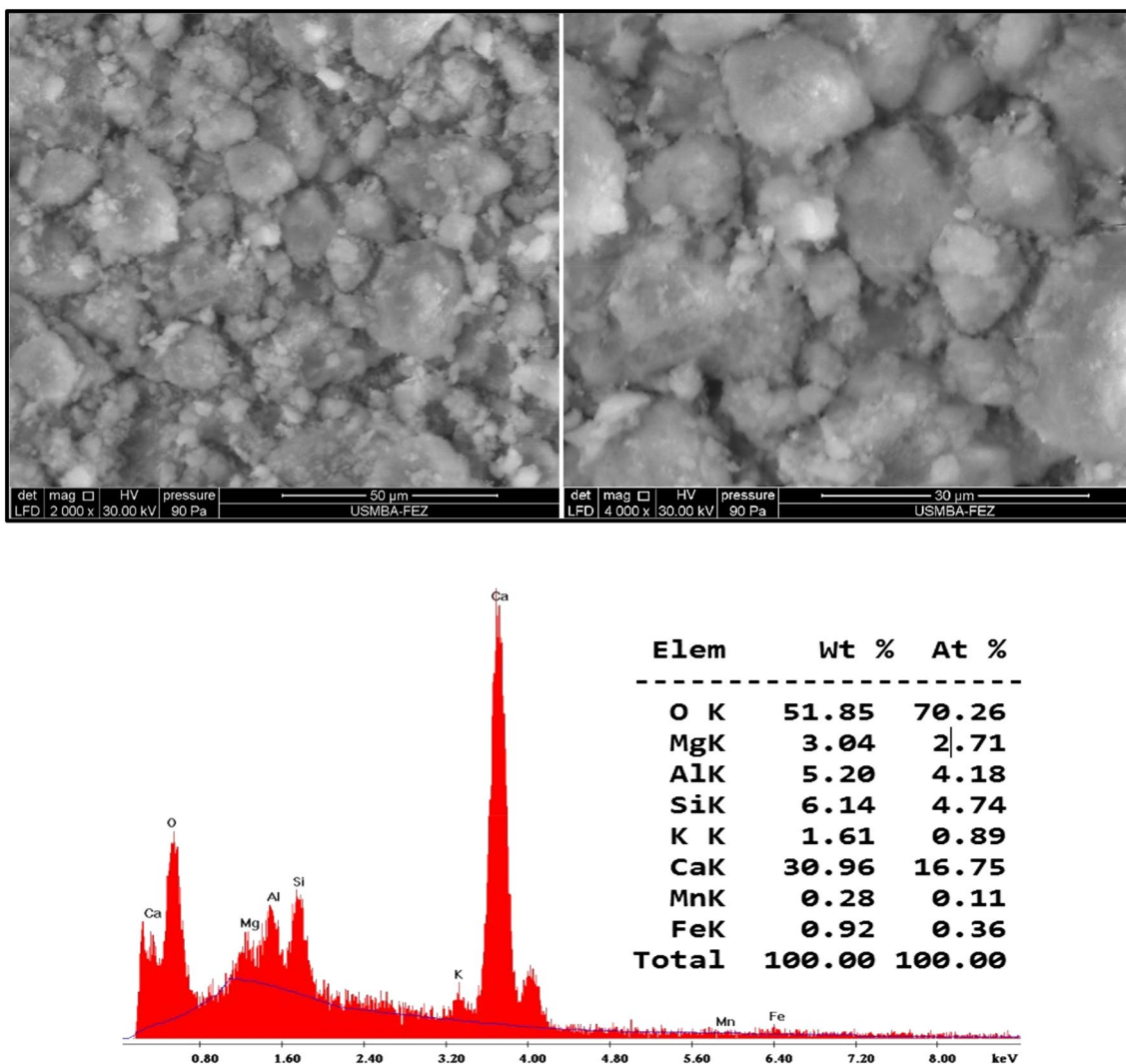


Fig. 5 SEM images and EDX microanalysis spectrum of the NMT

found that the equilibrium time for adsorbing these metal ions onto the NMT was 90 min and 180 min for Cr(VI) and Cu(II) ions, respectively, at room temperature. Adsorption capacities of 13.8 mg g^{-1} and 86.33 mg g^{-1} were observed for Cr(VI) and Cu(II) ions on the NMT, respectively. This trend is explained by the fact that, at the beginning of the process, the material contained a large number of vacant active sites for the Cr(VI) and Cu(II) ions. However, after a certain period of time, the surface was partially filled and the number of active sites available on the surface of the adsorbent decreased (Lairini et al. 2017).

Effect of pH

The solution pH has a remarkable influence on the adsorption efficiency. In fact, varying the pH alters the degree of ionization of the adsorbed ions, which changes the surface properties of the adsorbent (Lairini et al. 2017).

The percentages of the Cr(VI) and Cu(II) ions that are adsorbed as a function of pH at room temperature are presented in Fig. 7. The results show that the adsorption behavior of the adsorbent depends on the pH solution. As shown in Fig. 7a, the optimum adsorption is obtained at pH 6, with a removal efficiency of 91.31% and an adsorption capacity of 89.20 mg g^{-1} obtained for an adsorbent dose of 5 g L^{-1} , an initial Cu(II) concentration of 500 mg L^{-1} , and a contact time of 180 min. This can be attributed to the surface of the NMT, which contains a large number of active sites. For this reason, it becomes positively charged at low pH, leading to an increase in the competition between H^+ and Cu^{2+} metal ions for the available adsorption sites. However, as the pH increases, this competition decreases, as these active surface

sites become more negatively charged, which improves the adsorption of the positively charged metal ions through electrostatic attraction (Unuabonah et al. 2008; Yuan et al. 2019). Figure 7b shows that the optimal pH for Cr(VI) ion adsorption is 2, which yields a removal efficiency of 65.21% and an adsorption capacity of 16.30 mg g^{-1} with an initial Cr(VI) concentration of 50 mg L^{-1} and a contact time of 90 min. In aqueous solutions, $\text{H}_2\text{Cr}_2\text{O}_7$ can be observed at $\text{pH} < 1$, while the $\text{Cr}_2\text{O}_7^{2-}$ and HCrO_4^- species mostly exist at solution pH values of between 2 and 6. Above pH 6.8, only chromate (CrO_4^{2-}) is stable in solution, since little $\text{Cr}_2\text{O}_7^{2-}$ is present at low Cr(VI) concentrations such as 0.001 M under acid conditions. Therefore, Cr(VI) uptake in the present study occurred via the attraction of negatively charged HCrO_4^- ions to the highly protonated surface of the adsorbent. Since the highest protonation degree was obtained at pH 2, optimum adsorption occurred at pH 2. When the initial pH range was varied between 6 and 10, the protonation degree of the adsorbent surface gradually decreased, and the competition of the increasing number of $[\text{OH}^-]$ ions in the solution with the coexisting HCrO_4^- ions for the active surface sites also decreased the adsorption ability, thus decreasing the adsorption capacity. These results are in agreement with other studies.

Effect of adsorbent dose

The results for the effect of the adsorbent dose are shown in Fig. 8, and indicate the heavy metal removal efficiency (a) and the equilibrium heavy metal capacity (b) of the NMT at different dosages ranging from 1 to 10 g L^{-1} . As the adsorbent dose was increased, the removal efficiency

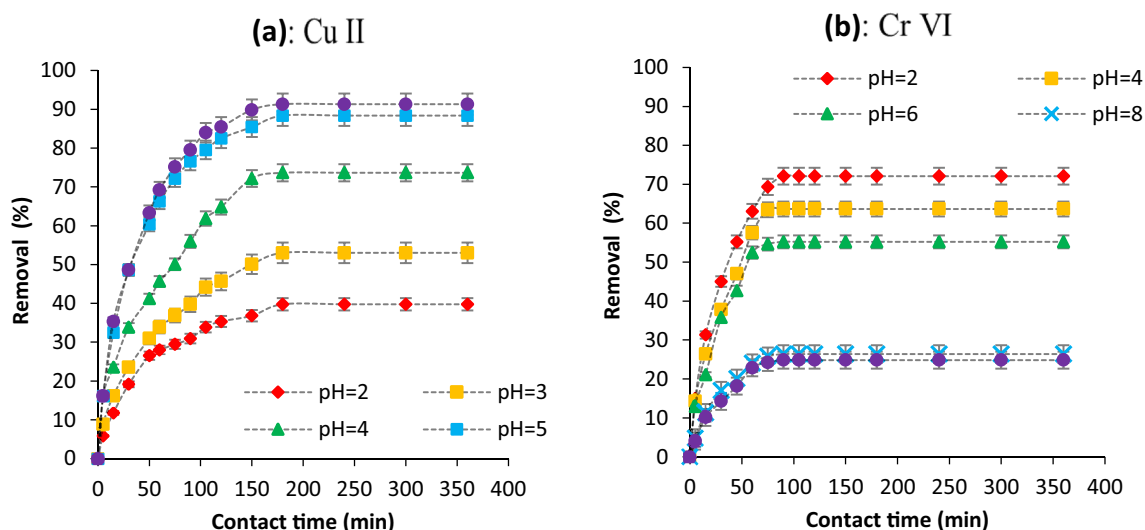


Fig. 7 Effect of pH on the removal of metal ions by NMT. **a** $[\text{Cu(II)}] = 500 \text{ mg L}^{-1}$, dose = 5 g L^{-1} , $T = 293 \pm 2 \text{ K}$. **b** $[\text{Cr(VI)}] = 50 \text{ mg L}^{-1}$, dose = 5 g L^{-1} , $T = 293 \pm 2 \text{ K}$

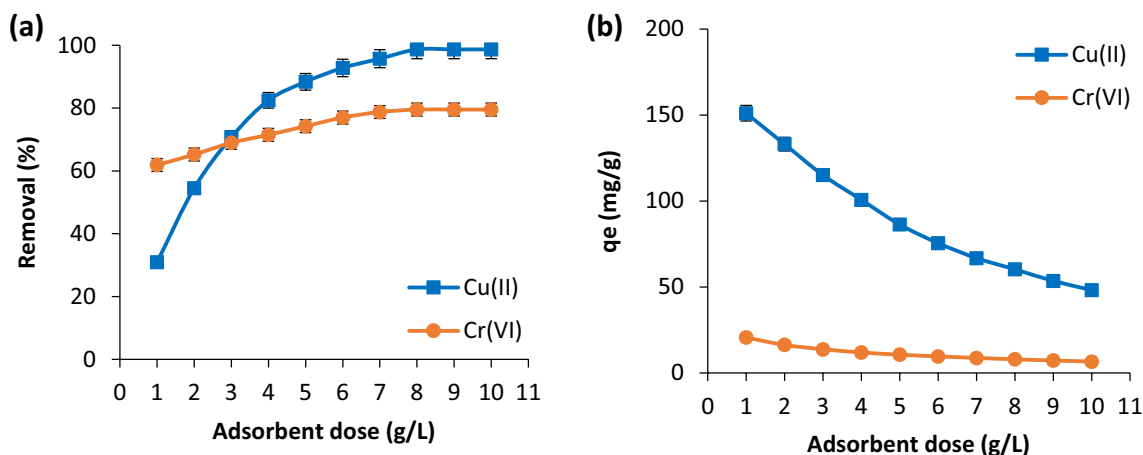


Fig. 8 Effect of NMT adsorbent dose on the adsorption of Cr(VI) and Cu(II). [Cu(II)]=500 mg L⁻¹, pH6, time=180 min, $T=293 \pm 2$ K. [Cr(VI)]=50 mg L⁻¹, pH2, time=90 min, $T=293 \pm 2$ K

increased from 61.88% to 79.52% for Cr(VI) ions and from 30.92 to 98.67% for Cu(II) ions, while the adsorption capacity decreased from 20.62 to 6.62 mg g⁻¹ and from 151.07 to 48.20 mg g⁻¹ for Cr(VI) and Cu(II) ions, respectively.

Many authors report that increasing the dose of the adsorbent provides more exchangeable sites or a larger contact surface, thus making contact between the metal ions and sorption sites easier.

Effect of initial metal concentration

The effect of the initial metal ion concentration on the removal of the metal ions is shown in Fig. 9a, b. The ion concentrations were varied in the range from 25 to 250 mg L⁻¹ for Cr(VI) ions and from 250 to 1750 mg L⁻¹ for Cu(II) ions. The removal of metal ions by the NMT decreased with increasing initial metal concentration. This was due to the high initial concentration of metal ions that were adsorbed

at the available sites; therefore, more metal ions were left unabsorbed in solution at higher concentration levels. An increase in the metal adsorption capacity with increasing initial metal concentration was observed, which was due to the driving force to overcome mass transfer resistance for metal ion transport between the solution and the surface of the adsorbent, as Arief et al. reported in their review of the biosorption of heavy metals from liquids (Arief et al. 2008).

Kinetic models

To gain insight into the adsorption mechanism, pseudo-first-order, pseudo-second-order, and Elovich kinetic models were considered. As can be seen in Table 3, the correlation coefficients (R^2) were higher for the pseudo-second-order model than for the pseudo-first-order model and the Elovich model, indicating that the pseudo-second-order equation was better at describing the adsorption kinetics of the Cr(VI) and

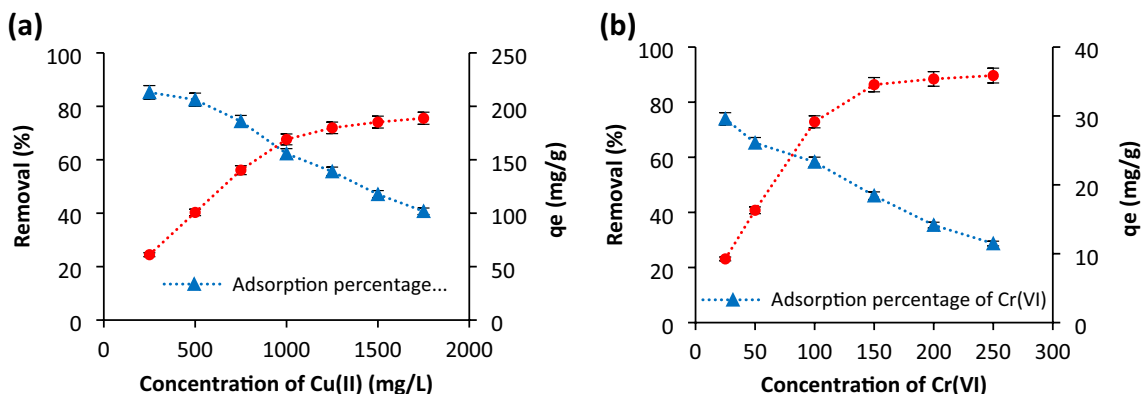


Fig. 9 Effect of the initial metal concentration on the removal of metal ions by NMT. **a** Cu(II); time=180 min, pH6, min, dose=3 g L⁻¹, $T=293 \pm 2$ K. **b** Cr(VI); time=90 min, pH2, dose=3 g L⁻¹, $T=293 \pm 2$ K

Table 3 Pseudo-first-order, pseudo-second-order, and Elovich kinetic model parameters for the adsorption of Cr(VI) and Cu(II) ions onto NMT at different temperatures

Metal ion	T (K)	q_e experimental (mg g ⁻¹)	Pseudo-first-order model		Pseudo-second-order model		Elovich model		
			$\ln(q_e - q_t) = \ln q_e - k_1 t$	R^2	$\frac{t}{q} = \frac{1}{k_2 q_e} + \frac{t}{q}$	R^2	$q_t = \frac{1}{\beta} \ln(\alpha \beta) + \frac{1}{\beta} \ln t$	α (mg g ⁻¹ min ⁻¹)	β (g mg ⁻¹)
Cr(VI)	298	29.14	2.61×10^{-2}	0.796	3.08×10^{-3}	0.997	0.050	0.122	0.994
	303	30.02	2.39×10^{-2}	0.896	2.98×10^{-3}	0.997	0.053	0.122	0.979
	313	30.17	3.48×10^{-2}	0.865	3.33×10^{-3}	0.997	0.047	0.115	0.986
Cu(II)	323	30.47	3.22×10^{-2}	0.787	3.32×10^{-3}	0.998	0.051	0.117	0.993
	298	140.28	0.96×10^{-2}	0.951	2.09×10^{-4}	0.995	0.107	0.037	0.974
	313	156.47	1.09×10^{-2}	0.933	2.71×10^{-4}	0.998	0.096	0.034	0.974
	323	165.46	1.06×10^{-2}	0.912	2.72×10^{-4}	0.998	0.106	0.031	0.966
	333	167.26	1.08×10^{-2}	0.923	2.93×10^{-4}	0.998	0.087	0.029	0.993

Cu(II) ions on the NMT. Furthermore, the calculated data (q_{cal}) for the pseudo-second-order model agree well with the experimental data (q_{exp}) (Assila et al. 2021; Dra et al. 2020a, b).

Pseudo-first-order model

Lagergren showed that the adsorption rate of an aqueous solution on an adsorbent is based on its adsorption capacity and follows a first-order equation. The nonlinear form of this first-order equation is (Bhattacharyya and Gupta 2011; Azzaz et al. 2018)

$$\frac{dq_t}{dt} = k_1(q_e - q_t), \tag{3}$$

where q_t (mg g⁻¹) is the adsorption capacity at time t , q_e (mg g⁻¹) is the equilibrium adsorption capacity, and k_1 (min⁻¹) is the first-order constant. After integration and applying the initial condition of $q=0$ at $t=0$, the equation takes the following form (Dehmani et al. 2020; Mejjad et al. 2016):

$$\ln(q_e - q_t) = \ln q_e - k_1 t. \tag{4}$$

The parameters k_1 and q_e can be calculated from the slope and intercept of a plot of $\log(q_e - q_t)$ versus t , and are given in Table 3. The resulting values of the correlation coefficient R^2 are low for the two metal ions. Furthermore, the measured experimental values of q_e are far from the calculated q_e values.

Pseudo-second-order model

The pseudo-second-order model was also used to describe the kinetics of the adsorption process. The pseudo-second-order kinetic model equation is expressed as follows:

$$\frac{dq_t}{dt} = k_2(q_e - q_t)^2. \tag{5}$$

Integration of this equation to $qt=0$ at $t=0$ yields the linear form

$$\frac{t}{q} = \frac{1}{k_2 q_e^2} + \frac{t}{q}, \tag{6}$$

where k_2 (g mg⁻¹ min⁻¹) is the pseudo-second-order rate constant. The kinetic parameters are given in Table 3. It is clear that the pseudo-second-order model represents the experimental data well ($R^2 \geq 0.995$). Besides, the calculated data (q_e calculated) agree well with the experimental data (q_e experimental). Similar results were found for the adsorption of Cu(II) ions on various adsorbents by several authors (Cao et al. 2014).

Elovich model

The Elovich equation is generally expressed as follows:

$$\frac{dq}{dt} = \alpha e^{-\beta q_t} \tag{7}$$

where q_t is the amount of metal ions at time t , and α and β are the initial metal ion sorption rate ($\text{mg g}^{-1} \text{min}^{-1}$) and the desorption constant (g mg^{-1}), respectively. Assuming that $\alpha\beta t \gg 1$ for simplicity, and applying the boundary conditions $qt=0$ at $t=0$ and $qT= q_t$ at $T=t$ to Eq. (7) yields

$$q_t = \frac{1}{\beta} \ln(\alpha\beta) + \frac{1}{\beta} \ln t. \tag{8}$$

Thus, the constants α and β can be obtained from the slope and intercept of the linear plot of q_t versus $\ln t$.

As seen in Table 3, the correlation coefficients (R^2) are higher for the pseudo-second-order model than for the pseudo-first-order model and the Elovich model, indicating that the pseudo-second-order equation is better at describing the adsorption kinetics of Cr(VI) and Cu(II) ions on the NMT. Furthermore, the calculated data (q_e calculated) for the pseudo-second-order model agree well with the experimental data (q_e experimental) (Amir 2015; Wang et al. 2017).

Intraparticle diffusion model

The mechanism of adsorbate uptake by the adsorbent and the reaction pathway for the adsorbate and adsorbent can be identified using the intraparticle diffusion model. Figure 10 describes the four steps associated with transport processes during adsorption by porous adsorbents: (i)

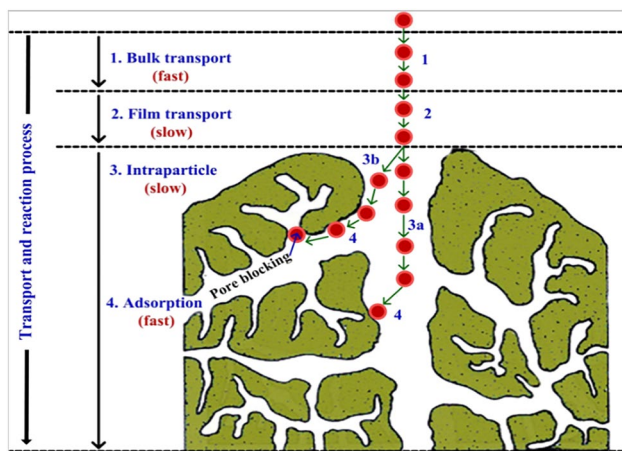


Fig. 10 Transport process during adsorption by a porous adsorbent

diffusion to the liquid film on the adsorbent surface, (ii) diffusion across the liquid film on the adsorbent surface, (iii) adsorption at the active sites on the surface, and (iv) diffusion of metal ions through pores of different sizes in the adsorbent particles (Pholosi et al. 2020; Gao et al. 2020; Bhattacharyya and Gupta 2006).

The linearized transformation of the intraparticle diffusion model is given by

$$q_t = k_p t + C, \tag{9}$$

where

- k_p ($\text{mg g}^{-1} \text{min}$) is the rate constant in the intraparticle diffusion model
- C (mg g^{-1}) is a constant associated with the thickness of the boundary layer.

According to this model, if a plot of q_t versus $t_{1/2}$ gives a straight line, the adsorption process is controlled by intraparticle diffusion; if the data yield a multilinear plot, two or more steps control the adsorption process.

Figures 11 and 12 show the intraparticle diffusion plots for Cu and Cr(VI) adsorption onto NMT, respectively. For both of the studied cations, the results of this research show that the plot presents two distinct linear portions, which means that adsorption is not controlled by intraparticle diffusion only (Zsirka et al. 2016).

The first linear portion is due to external surface adsorption, in which the uptake rate of chromium ions is high due to the film diffusion of Cr(VI) through the solution onto the external surface of the NMT. The second linear portion, which is less steep, refers to slow intraparticle pore diffusion. Therefore, the adsorption process of Cr(VI) and Cu(II) is controlled by two steps: external film and intraparticle pore diffusion (Copaja et al. 2020; Soltanian 2015).

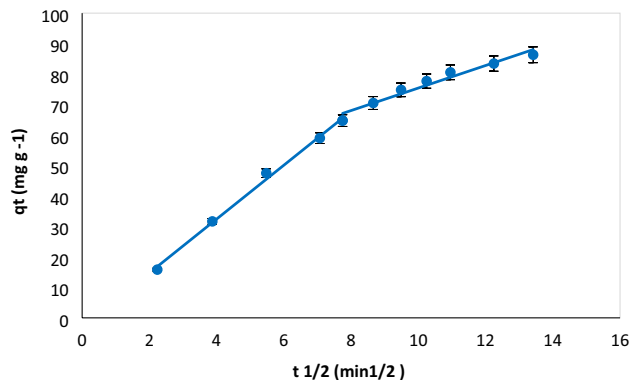


Fig. 11 Intraparticle diffusion plot of Cu (500 mg L^{-1}) adsorption onto NMT

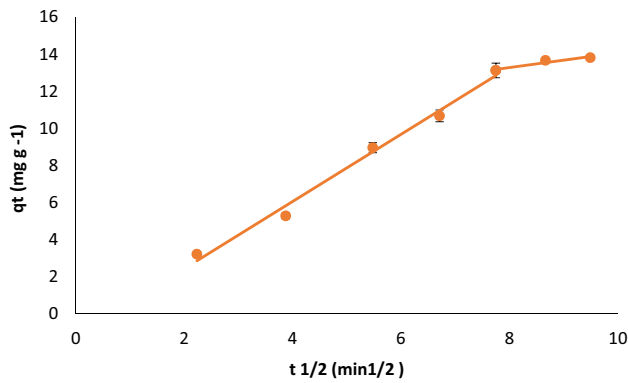


Fig. 12 Intraparticle diffusion plot of Cr(VI) (50 mg L^{-1}) adsorption onto NMT

Isotherm models

Langmuir isotherm

Adsorption isotherms describe and explain the correlation between the adsorbent and adsorbate, which is important for optimizing the adsorption process. In this study, some commonly used isotherm models such as the Langmuir, Freundlich, and Dubinin–Radushkevich (D–R) models were applied to fit the obtained experimental data. An adsorption isotherm should be given as the equilibrium adsorbed amount versus the equilibrium ion concentration for a constant equilibrium solution pH and temperature (Günay et al. 2007).

Monolayer adsorption processes and adsorption at specific homogeneous sites on the adsorbent are assumptions upon which the Langmuir model is based (Langmuir 1918; Benjelloun et al. 2021).

The linear form of the Langmuir equation is

$$\frac{C_e}{q_e} = \frac{C_e}{q_m} + \frac{1}{K_L q_m}, \quad (10)$$

where K_L is the Langmuir constant (L mg^{-1}) and q_m (mg/g) represents the maximum adsorption capacity under experimental conditions, and q_m and K_L are determined from the plot of C_e/q_e as a function of C_e (Fig. 13).

Using the Langmuir constant, the dimensionless separation factor R_L is given by

$$R_L = \frac{1}{(1 + K_L C_0)}, \quad (11)$$

where R_L is related to the nature of the adsorbent/adsorbate interaction and the isotherm type: irreversible ($R_L = 0$), favorable ($0 < R_L < 1$), linear ($R_L = 1$), or unfavorable ($R_L > 1$) (Shi et al. 2009). $0.086 \leq R_L \leq 0.321$ and $0.059 \leq R_L \leq 0.257$

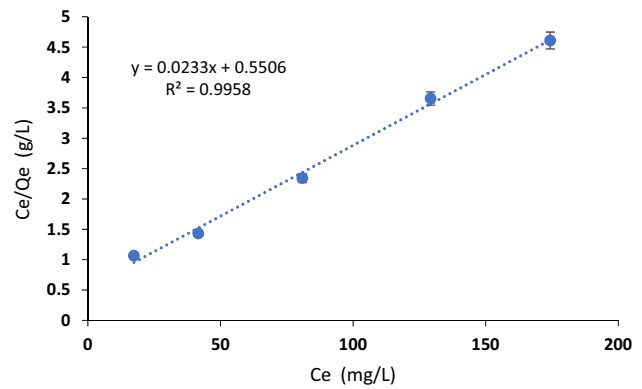


Fig. 13 Langmuir isotherm model

for Cr(VI) and Cu(II) ions, respectively, indicate highly favorable Langmuir adsorption at a high initial metal ion concentration.

Figure 13 shows the Langmuir isotherm model presented by the correlation between C_e/q_e and C_e , while the corresponding parameters are presented in Table 4.

Freundlich isotherm

The Freundlich model can be applied to nonideal sorption on heterogeneous surfaces and multilayer sorption. The linear form of the equation of Freundlich can be written in the following logarithmic form:

$$\log q_e = \log K_F + \frac{1}{n} \log C_e, \quad (12)$$

where K_F and $1/n$ are the Freundlich constants, which are connected to the adsorption capacity and the intensity of adsorption of the adsorbent, respectively.

The Freundlich isotherm model is presented in Fig. 14, and the obtained parameters are summarized in Table 4.

Dubinin–Radushkevich (D–R) isotherm

The D–R model was also applied to the equilibrium data to determine if the adsorption occurred by physical or chemical processes. The linearized form of the D–R isotherm is as follows:

$$\ln q_e = \ln q_{mDR} - K_{DR} \varepsilon^2 \quad (13)$$

$$\varepsilon = RT \ln \frac{C_s}{C_e}, \quad (14)$$

where q_{mDR} is the maximum adsorption capacity of the adsorbent (mg g^{-1}), R is the gas constant (8.314 J mol^{-1})

Table 4 Parameters of isotherm models for the adsorption of Cr(VI) and Cu(II) ions onto NMT

Metal ion	Langmuir			Freundlich			Dubinin–Radushkevich			
	q_m	K_L	R^2	n	K_F	R^2	q_m	K_{DR}	E	R^2
Cr(VI)	42.91	4.23×10^{-2}	0.995	0.395	0.012	0.880	35.43	40.913	0.111	0.991
Cu(II)	208.33	1.05×10^{-2}	0.999	2.76	18.31	0.930	131.81	287.55	0.041	0.905

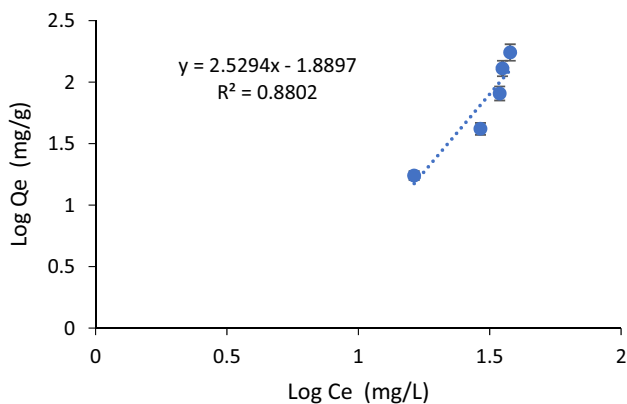


Fig. 14 Freundlich isotherm model

K^{-1} , T is the temperature (K), K_{DR} is the Dubinin–Radushkevich constant ($\text{mol}^2 \text{kJ}^{-2}$), and ε is the Polanyi potential (J mol^{-1}) (Dada et al. 2012).

If a linear relationship is obtained between $\ln q_e$ and ε^2 , the values of K_{DR} and q_m can be determined. The mean free energy of adsorption, E (kJ mol^{-1}), can then be calculated from K_{DR} with the following equation:

$$E = \frac{1}{\sqrt{2K_{DR}}} \tag{15}$$

This adsorption potential is independent of the temperature, but it varies depending on the nature of the adsorbent and adsorbate. The mean free energy of adsorption E gives information about the adsorption mechanism (chemical ion exchange or physical adsorption). If the E value is between 8 and 16 kJ mol^{-1} , the adsorption process proceeds by chemical ion exchange; if $E < 8 \text{ kJ mol}^{-1}$, the adsorption process is physical in nature. The mean adsorption energy E was calculated to be 0.111 kJ mol^{-1} for the adsorption of Cr(VI) ions and 0.041 kJ mol^{-1} for the adsorption of Cu(II) ions onto NMT (Table 4). These results indicate

that the adsorption of the metal ions onto NMT may occur via physical adsorption. Similar results for the adsorption of Cr(VI) and Cu(II) ions onto natural materials have been reported from other studies (Charriau et al. 2011).

Adsorption thermodynamics

The thermodynamic parameters of the adsorption isotherm are the free energy (ΔG°), the enthalpy (ΔH°), and the entropy (ΔS°). These parameters were determined from the experimental data using the following equations:

$$K_c = \frac{q_e}{C_e} \tag{16}$$

$$\Delta G^\circ = -RT \ln K_c \tag{17}$$

$$\Delta G^\circ = \Delta H^\circ - T \Delta S^\circ \tag{18}$$

$$\ln K_c = \frac{\Delta S^\circ}{R} - \frac{\Delta H^\circ}{RT}, \tag{19}$$

where K_c is the equilibrium constant, q_e (mg g^{-1}) is the equilibrium adsorption capacity, and C_e (mg L^{-1}) is the equilibrium concentration of the adsorbate.

According to Eq. (19), the parameters ΔH° and ΔS° can be calculated from the slope and intercept, respectively, of a plot of $\ln K_c$ versus $1/T$, where $\Delta H^\circ/R$ is the slope and $\Delta S^\circ/R$ is the ordinate of the origin (Veli et al. 2007).

The negative ΔG° values of the Cu(II) ions indicate that the adsorption of Cu(II) ions on NMT is feasible and spontaneous, and the value of ΔG° becomes more negative with increasing temperature, indicating that a higher temperature facilitates the adsorption of Cu(II) ions onto natural material due to a greater driving force for adsorption (Table 5). Also, the ΔH° values are smaller than the lower limit of chemisorption, which is 42 kJ/mol , which means that the Cr(VI)

Table 5 Thermodynamic parameters of the adsorption of Cr(VI) and Cu(II) ions onto NMT

Metal ion	ΔG° (kJ mol^{-1})				ΔH° (kJ mol^{-1})	ΔS° ($\text{J mol}^{-1} \text{K}^{-1}$)
	$T=298 \text{ K}$	$T=303 \text{ K}$	$T=313 \text{ K}$	$T=323 \text{ K}$		
Cr(VI)	0.867	0.7832	0.727	0.671	2.536	5.601
Cu(II)	-15.74	-17.965	-19.449	-20.933	28.477	148.38

and Cu(II) ions are adsorbed onto the NMT via physisorption (Azzaz et al. 2015; Dehmani et al. 2020).

However, the positive values of ΔG° for the adsorption of Cr(VI) ions onto NMT suggest that the conversion of the reactants into products requires a small amount of energy. This may not suggest that the reaction is not spontaneous; rather, it could indicate that it will perform better when the solution temperature is increased to 323 K (Copaja et al. 2020).

Conclusion

The objective of this work was to study the potential of a natural material from Morocco to act as an adsorbent for two heavy metals in aqueous solutions. Experimental parameters such as the contact time, solution pH, adsorbent dose, and initial concentration were optimized to obtain the highest possible removal of Cr(VI) and Cu(II) ions using this adsorbent. Batch studies clearly suggest that the maximum adsorption yield is 91.31% for Cu(II) ion adsorption onto NMT at pH 6 and 65.21% for Cr(VI) ion adsorption at pH 2. The adsorption kinetics match well with the pseudo-second-order model for both heavy metals, and the adsorption isotherms are well represented by the Langmuir model. The adsorption process was spontaneous for the removal of Cu(II), and the positive values of the standard enthalpy change showed the endothermic and physical nature of the adsorption. The results show that this natural material is an environmentally friendly and effective material for adsorbing Cr(VI) and Cu(II) from an aqueous solution.

Declarations

Conflict of interest The authors declare that there is no conflict of interest regarding the publication of this paper.

References

- AbouZakhem B, Hafez R (2015) Heavy metal pollution index for groundwater quality assessment in Damascus Oasis, Syria. *Environ Earth Sci* 73:6591–6600. <https://doi.org/10.1007/s12665-014-3882-5>
- Amar M, Benzerzour M, Kleib J, Abriak NE (2021) From dredged sediment to supplementary cementitious material: characterization, treatment, and reuse. *Int J Sediment Res* 36:92–109. <https://doi.org/10.1016/j.ijsrc.2020.06.002>
- Amir S (2015) Contribution à la valorisation de boues de stations d'épuration par compostage: devenir des micropolluants métalliques et organiques et bilan humique du compost. Soumia Amir, University Polytechnic Toulouse, France. <https://www.semanticscholar.org/paper/Contribution-%C3%A0-la-valorisation-de-boues-de-stations-Amir/5f216050ce63fba308b5e1b76a8de5d6ba06f72c>
- Annadurai G, Juang RS, Lee DJ (2003) Adsorption of heavy metals from water using banana and orange peels. *Water Sci Technol* 47:185–190. <https://doi.org/10.2166/WST.2003.0049>
- Arief VO, Trilestari K, Sunarso J et al (2008) Recent progress on biosorption of heavy metals from liquids using low cost biosorbents: characterization, biosorption parameters and mechanism studies. *Clean Soil Air Water* 36:937–962. <https://doi.org/10.1002/clen.200800167>
- Assila O, Zouheir M, Tanji K et al (2021) Copper nickel co-impregnation of Moroccan yellow clay as promising catalysts for the catalytic wet peroxide oxidation of caffeine. *Heliyon* 7:e06069. <https://doi.org/10.1016/j.heliyon.2021.e06069>
- Azzaz AA, Jellali S, Assadi AA, Bousselmi L (2015) Chemical treatment of orange tree sawdust for a cationic dye enhancement removal from aqueous solutions: kinetic, equilibrium and thermodynamic studies. *New Pub Balaban* 57:22107–22119. <https://doi.org/10.1080/19443994.2015.1103313>
- Azzaz AA, Jellali S, Akrou H et al (2018) Dynamic investigations on cationic dye desorption from chemically modified lignocellulosic material using a low-cost eluent: dye recovery and anodic oxidation efficiencies of the desorbed solutions. *J Clean Prod* 201:28–38. <https://doi.org/10.1016/J.JCLEPRO.2018.08.023>
- Bayou J, Abdullai M, Kenneth A, Pelig B (2020) Desorption of chromium (VI) and lead (II) ions and regeneration of the exhausted adsorbent. *Appl Water Sci* 10:1–6. <https://doi.org/10.1007/s13201-020-01250-y>
- Benjelloun M, Miyah Y, AkdemirEvrendilek G et al (2021) Recent advances in adsorption kinetic models: their application to dye types. *Arab J Chem* 14:103031. <https://doi.org/10.1016/j.arabjc.2021.103031>
- Bhattacharyya KG, Sen GS (2011) Removal of Cu(II) by natural and acid-activated clays: an insight of adsorption isotherm, kinetic and thermodynamics. *Desalination* 272:66–75. <https://doi.org/10.1016/j.desal.2011.01.001>
- Bohli T, Ouederni A, Villaescusa I (2017) Simultaneous adsorption behavior of heavy metals onto microporous olive stones activated carbon: analysis of metal interactions. *Euro Mediterr J Environ Integr* 2:1–15. <https://doi.org/10.1007/s41207-017-0030-0>
- Booker NA, Cooney EL, Priestley AJ (1996) Ammonia removal from sewage using natural Australian zeolite. *Water Sci Technol* 34:17–24. [https://doi.org/10.1016/S0273-1223\(96\)00782-2](https://doi.org/10.1016/S0273-1223(96)00782-2)
- Burakov AE, Galunin EV, Burakova IV et al (2018) Adsorption of heavy metals on conventional and nanostructured materials for wastewater treatment purposes: a review. *Ecotoxicol Environ Saf* 148:702–712. <https://doi.org/10.1016/J.ECOENV.2017.11.034>
- Campodonico VA, García MG, Pasquini AI (2015) The dissolved chemical and isotopic signature downflow the confluence of two large rivers: the case of the Parana and Paraguay rivers. *J Hydrol* 528:161–176. <https://doi.org/10.1016/j.jhydrol.2015.06.027>
- Cao JS, Lin JX, Fang F et al (2014) A new adsorbent by modifying walnut shell for the removal of anionic dye: kinetic and thermodynamic studies. *Bioresour Technol* 163:199–205
- Charriau A, Lesven L, Gao Y et al (2011) Trace metal behaviour in riverine sediments: role of organic matter and sulfides. *Appl Geochem* 26:80–90. <https://doi.org/10.1016/j.apgeochem.2010.11.005>
- Copaja SV, Mauro L, Vega-retter C, Véliz D (2020) Adsorption-desorption of trace elements in sediments of the Maipo River basin. *J Chil Chem Soc* 2:4778
- Dada AO, Olalekan AP, Olatunya AM et al (2012) Langmuir, Freundlich, Temkin and Dubinin–Radushkevich isotherms studies of equilibrium sorption of Zn²⁺ onto phosphoric acid modified rice husk. 3:38–45
- Dehmani Y, Ed-Dra A, Zennouhi O et al (2020) Chemical characterization and adsorption of oil mill wastewater on Moroccan clay

- in order to be used in the agricultural field. *Heliyon* 6:e03164. <https://doi.org/10.1016/j.heliyon.2020.e03164>
- Dra A, El Gaidoumi A, Tanji K et al (2019) Characterization and quantification of heavy metals in oued sebou sediments. *Sci World J* 2019:21–23. <https://doi.org/10.1155/2019/7496576>
- Dra A, Tanji K, Arrahli A et al (2020a) Valorization of oued sebou natural sediments (Fez-Morocco area) as adsorbent of methylene blue dye: kinetic and thermodynamic study. *Sci World J* 2020:8. <https://doi.org/10.1155/2020/2187129>
- Dra A, Tanji K, Arrahli A et al (2020b) Corrigendum to “Valorization of oued sebou natural sediments (Fez-Morocco area) as adsorbent of methylene blue dye: kinetic and thermodynamic study.” *Sci World J* 2020:4815767. <https://doi.org/10.1155/2020/4815767>
- El Gaidoumi A, Loqman A, Zouheir M et al (2021) Sol–gel fluorinated TiO₂-clay nanocomposite: study of fluor-titanium interaction on the photodegradation of phenol. *Res Chem Intermed* 47:1–26. <https://doi.org/10.1007/s11164-021-04573-w>
- El Mrabet I, Nawdali M, Rafqah S et al (2020) Low-cost biomass for the treatment of landfill leachate from Fez City: application of a combined coagulation–adsorption process. *Euro Mediterr J Environ Integr* 5:14. <https://doi.org/10.1007/s41207-020-00201-y>
- Gao Z, Guo H, Zhao B et al (2020) Experiment-based geochemical modeling of arsenic(V) and arsenic(III) adsorption onto aquifer sediments from an inland basin. *J Hydrol* 588:125094. <https://doi.org/10.1016/j.jhydrol.2020.125094>
- Günay A, Arslankaya E, Tosun I (2007) Lead removal from aqueous solution by natural and pretreated clinoptilolite: adsorption equilibrium and kinetics. *J Hazard Mater* 146:362–371. <https://doi.org/10.1016/j.jhazmat.2006.12.034>
- Jeguirim M, Limousy L (2019) Biomass chars: elaboration, characterization and applications II. *Energies* 12:384. <https://doi.org/10.3390/en12030384>
- Kamagate M, Assadi AA, Kone T et al (2018) Use of laterite as a sustainable catalyst for removal of fluoroquinolone antibiotics from contaminated water. *Chemosphere* 195:847–853. <https://doi.org/10.1016/j.chemosphere.2017.12.165>
- Lairini S, El Mahtal K, Miyah Y et al (2017) The adsorption of crystal violet from aqueous solution by using potato peels (*Solanum tuberosum*): equilibrium and kinetic studies. *J Mater Environ Sci* 8:3252–3261
- Langmuir I (1918) The adsorption of gases on plane surfaces of glass, mica and platinum. *J Am Chem Soc* 345:1361–1403
- Magali S (2008) Spéciation du cadmium, du plomb et du zinc dans les poussières d'émissions atmosphériques d'origine sidérurgique - Approche de l'impact toxicologique des poussières. - document
- Mejjad N, Laïssaoui A, El-Hammoumi O et al (2016) Sediment geochronology and geochemical behavior of major and rare earth elements in the Oualidia Lagoon in the western Morocco. *J Radioanal Nucl Chem* 309:1133–1143. <https://doi.org/10.1007/s10967-016-4714-8>
- Motsi T, Rowson NA, Simmons MJH (2009) Adsorption of heavy metals from acid mine drainage by natural zeolite. *Int J Miner Process* 92:42–48. <https://doi.org/10.1016/j.minpro.2009.02.005>
- Olusegun SJ, de Sousa Lima LF, Mohallem NDS (2018) Enhancement of adsorption capacity of clay through spray drying and surface modification process for wastewater treatment. *Chem Eng J* 334:1719–1728. <https://doi.org/10.1016/j.cej.2017.11.084>
- Panda L, Das B, Rao DS, Mishra BK (2011) Application of dolochar in the removal of cadmium and hexavalent chromium ions from aqueous solutions. *J Hazard Mater* 192:822–831. <https://doi.org/10.1016/j.jhazmat.2011.05.098>
- Pholosi A, Naidoo EB, Ofomaja AE (2020) Intraparticle diffusion of Cr(VI) through biomass and magnetite coated biomass: a comparative kinetic and diffusion study. *South Afr J Chem Eng* 32:39–55. <https://doi.org/10.1016/j.sajce.2020.01.005>
- Qu Z, Dong G, Zhu S et al (2020) Recycling of groundwater treatment sludge to prepare nano-rod erdite particles for tetracycline adsorption. *J Clean Prod* 257:120462. <https://doi.org/10.1016/j.jclepro.2020.120462>
- Riffi SA, Hte R (2013) Gerer le reseau d'assainissement de la ville de fes valoriser collecter, traiter
- Saltali K, Sari A, Aydin M (2007) Removal of ammonium ion from aqueous solution by natural Turkish (Yıldızeli) zeolite for environmental quality. *J Hazard Mater* 141:258–263. <https://doi.org/10.1016/j.jhazmat.2006.06.124>
- Šćiban M, Radetić B, Kevrešan Ž, Klačnja M (2007) Adsorption of heavy metals from electroplating wastewater by wood sawdust. *Bioresour Technol* 98:402–409. <https://doi.org/10.1016/j.biortech.2005.12.014>
- Shi T, Jia S, Chen Y et al (2009) Adsorption of Pb(II), Cr(III), Cu(II), Cd(II) and Ni(II) onto a vanadium mine tailing from aqueous solution. *J Hazard Mater* 169:838–846. <https://doi.org/10.1016/j.jhazmat.2009.04.020>
- Soltanian MR (2015) Relating reactive transport to hierarchical and multiscale relating reactive transport to hierarchical and multiscale sedimentary architecture. PhD thesis. <https://doi.org/10.13140/RG.2.1.4718.6083>
- Tournassat C, Bourg IC, Steefel CI, Bergaya F (2015) Surface properties of clay minerals. *Dev Clay Sci* 6:5–31. <https://doi.org/10.1016/B978-0-08-100027-4.00001-2>
- Uddin MK (2017) A review on the adsorption of heavy metals by clay minerals, with special focus on the past decade. *Chem Eng J* 308:438–462. <https://doi.org/10.1016/j.cej.2016.09.029>
- Unuabonah EI, Adebowale KO, Olu-Owolabi BI et al (2008) Adsorption of Pb(II) and Cd(II) from aqueous solutions onto sodium tetraborate-modified kaolinite clay: equilibrium and thermodynamic studies. *Hydrometallurgy* 93:1–9. <https://doi.org/10.1016/j.hydromet.2008.02.009>
- Veli S, Alyüz B, Aly B (2007) Adsorption of copper and zinc from aqueous solutions by using natural clay. *J Hazard Mater* 149:226–233. <https://doi.org/10.1016/j.jhazmat.2007.04.109>
- Wang Z, Li X, Liang H et al (2017) Equilibrium, kinetics and mechanism of Au³⁺, Pd²⁺ and Ag⁺ ions adsorption from aqueous solutions by graphene oxide functionalized persimmon tannin. *Mater Sci Eng C* 79:227–236. <https://doi.org/10.1016/j.msec.2017.05.038>
- Wang HY, Göttlicher J, Byrne JM et al (2021) Vertical redox zones of Fe–S–As coupled mineralogy in the sediments of Hetao Basin – constraints for groundwater As contamination. *J Hazard Mater* 408. <https://doi.org/10.1016/j.jhazmat.2020.124924>
- Yuan S, Tang H, Xiao Y et al (2019) Phosphorus contamination of the surface sediment at a river confluence. *J Hydrol* 573:568–580. <https://doi.org/10.1016/j.jhydrol.2019.02.036>
- Zsirka B, Horváth E, Járvas Z et al (2016) Applied clay science structural and energetical characterization of exfoliated kaolinite surfaces. *Appl Clay Sci* 124–125:54–61. <https://doi.org/10.1016/j.clay.2016.01.035>